arXiv:1906.09212v1 [cond-mat.mes-hall] 21 Jun 2019

Breathing Mode of a Skyrmion on a Lattice

Dmitry A. Garanin[1], Reem Jaafar[2], and Eugene M. Chudnovsky[1]
[1] *Physics Department, Herbert H. Lehman College and Graduate School, The City University of New York, 250 Bedford Park Boulevard West, Bronx, New York 10468-1589, USA*
[2] *Department of Mathematics, Engineering and Computer Science, LaGuardia Community College, The City University of New York, 31-10 Thomson Avenue, Long Island City, NY 11101*

(Dated: February 1, 2022)

The breathing mode of a skyrmion, corresponding to coupled oscillations of its size and chirality angle is studied numerically for a conservative classical-spin system on a 500×500 lattice. The dependence of the oscillation frequency on the magnetic field is computed. It is linear at small fields, reaches maximum on increasing the field, then sharply tends to zero as the field approaches the threshold above which the skyrmion loses stability and collapses. Physically transparent analytical model is developed that explains the results qualitatively and provides the field dependence of the oscillation frequency that is close to the one computed numerically. It is shown that a large-amplitude breathing motion in which the skyrmion chirality angle γ is rotating in one direction is strongly damped and quickly ends by the skyrmion collapse. To the contrary, smaller-amplitude breathing motion in which γ oscillates is undamped.

I. INTRODUCTION

Studies of skyrmions have opened a promising avenue for developing new forms of memory storage and information processing [1–7]. Skyrmions in thin films are defects of the uniformly magnetized ferromagnetic state stabilized by topology. They had been first introduced in the non-linear σ-model by Skyrme [8] and later intensively studied in nuclear physics [9]. Their topological properties in a two-dimensional (2D) Heisenberg exchange model have been elucidated by Belavin and Polyakov (BP) [10, 11]. In practice, topological stability of skyrmions that arises from the continuous field model is violated in solids by the discreteness of the atomic lattice [12]. External magnetic field, magnetic anisotropy, dipole-dipole interaction (DDI), thermal and quantum fluctuations, etc., further break the symmetry of the exchange model, leading to the uncontrolled collapse or expansion of skyrmions. For that reason they are typically observed in non-centrosymmetric materials. In such materials the Dzyaloshinskii-Moriya interaction (DMI) that arises from the lack of the inversion symmetry provides stability of skyrmions within a certain area of the phase diagram [5, 13]. To date, stable isolated skyrmions have been experimentally observed at room temperatures [7, 14, 15]. It has been demonstrated that the size of a skyrmion can be tuned by the external magnetic field, with its radius shrinking on increasing the field opposite to the skyrmion's spin until the skyrmion disappears [16, 17].

The shape of the smallest skyrmions is typically close to the shape provided by the BP solution of the pure exchange model [20], while bigger skyrmions resemble magnetic bubbles studied in the past [21]. Field-theoretical approach to the internal dynamics of skyrmions in nuclear physics and 2D magnets goes back to 1980s [18, 19]. More recently the interest to the internal modes of skyrmions stabilized by the DMI has developed [22]. Chiral spin-wave modes of skyrmions and edge oscillations of skyrmion bubbles, including a breathing-type mode, have been predicted [23, 24] and experimentally observed [25] in skyrmion crystals. A translational mode and different type of breathing modes have been calculated for isolated skyrmions using Landau-Lifshitz-Gilbert (LLZ) dynamics in Ref. [26]. Hybridization of breathing modes with quantized spin-wave modes in circular ultrathin magntic dots have been investigated via micromagnetic computations [27]. Contribution of the internal modes to the mass of a skyrmion bubble has been studied [28, 29]. Most recently, LLZ dissipative breathing dynamics of skyrmions and antiskyrmions has been analyzed within Hamiltonian formalism [30].

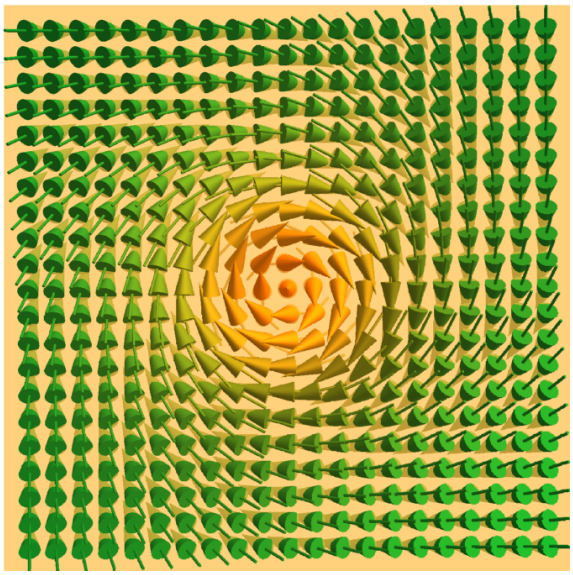


FIG. 1: Spin field in a Bloch-type skyrmion studied in the paper. Its breathing mode corresponds to the coupled oscillations of the skyrmion size and spin angles.

In this paper we focus on the problem that has not been previously addressed: excitation spectrum of small skyrmions close to their stability threshold. The breathing mode of a skyrmion shown in Fig. 1 is investigated. It corresponds to coupled oscillations of the skyrmion size and spin angles. We will show that the frequency of the mode has a distinct behavior in the collapse region that must be possible to detect in experiment. It is linear on the field at weak fields, riches maximum in the critical region and tends to zero as the field approaches the collapse threshold. Close behavior has been obtained by two independent methods. The first method consists of a purely numerical computation of the spin dynamics on 2D lattices of size ranging from 100×100 to 500×500, with a check that the results are independent on the size in the limit of a large lattice. The frequency of that internal skyrmion mode is below the spin-wave spectrum of the uniformly magnetized ferromagnetic state, explaining why no dissipation of the breathing mode has been observed in the numerical experiment. The second method uses analytical and semi-analytical models based upon Lagrangian dynamics of the skyrmion. It provides a transparent physical picture of the behavior of the breathing mode on the magnetic field. Quantitative agreement of the analytical method with numerical calculation on the lattice is within 20%.

The paper is structured as follows. The model, the numerical method, and the results for the small-amplitude skyrmion breathing mode computed on a lattice are given in Section II. Section III contains one crude qualitative approach and another more refined semi-analytical approach to skyrmion internal oscillations that provide clear physical interpretation of the numerical results. Dynamics of large-amplitude breathing modes is considered in Sec. IV. Our conclusions are summarized in Section V.

II. SKYRMION BREATHING MODE IN THE LATTICE MODEL

A. General

We consider a two-dimensional square lattice of normalized classical spins, $\mathbf{s}_i \equiv \mathbf{S}_i/S$ where $\mathbf{S}_i$ is a three-dimensional vector and $i=\{i_x,i_y\}$ refers to the lattice site. The Hamiltonian of the system is given by

$$\begin{aligned}\mathcal{H} &= -\frac{S^2}{2}\sum_{ij}J_{ij}\mathbf{s}_i\cdot\mathbf{s}_j - HS\sum_i s_{iz} - \frac{DS^2}{2}\sum_i s_{iz}^2 \\ &- AS^2\sum_i\left[(\mathbf{s}_i\times\mathbf{s}_{i+\delta_x})\cdot\mathbf{e}_x + (\mathbf{s}_i\times\mathbf{s}_{i+\delta_y})\cdot\mathbf{e}_y\right]. \quad (1)\end{aligned}$$

The first term represents the Heisenberg exchange energy with the exchange constant J and sum is taken over the nearest neighbors. The second term is the Zeeman interaction energy due to the external field H normal to the xy plane. The third term is the energy of the perpendicular magnetic anisotropy (PMA) of strength D. The last term represents the Dzyaloshinskii-Moriya interaction (DMI) of strength A, and $\mathbf{s}_{i+\delta_x}=\mathbf{s}_{i_x\pm1,i_y}$, etc. For certainty, we have chosen the Bloch type DMI that favors the Bloch-type skyrmions shown in Fig. 1.

The presence of the skyrmion in the system is revealed by a nonzero topological charge:

$$Q=\frac{1}{4\pi}\int dxdy\ \mathbf{s}\cdot\left(\frac{\partial\mathbf{s}}{\partial x}\times\frac{\partial\mathbf{s}}{\partial y}\right) \quad (2)$$

that takes discrete values $Q=0,\pm1,\pm2,...$ In numerical work we compute the discretized version of this expression.

Within the purely exchange continuous model, the BP solution for the skyrmion with $Q=1$ and spins in the center of the skyrmion pointing up against the spin-down background in terms of polar coordinates $x=r\cos\phi$, $y=r\sin\phi$ has the form

$$\left\{\begin{array}{c}s_x\\ s_y\end{array}\right\}=\frac{2\lambda r}{r^2+\lambda^2}\left\{\begin{array}{c}\cos(\phi+\gamma)\\ \sin(\phi+\gamma)\end{array}\right\},\quad s_z=\frac{\lambda^2-r^2}{\lambda^2+r^2}. \quad (3)$$

Here λ is the skyrmion size and spins are rotated away from the radial direction by the chirality angle γ. The energy of the skyrmion is independent of λ and γ and equal to $4\pi JS^2$ above that of the uniform state. This is the invariance found by Belavin and Polyakov.

It was shown that the discreteness of the lattice makes the energy decrease with decreasing λ that leads to the skyrmion collapse [12]. Other interactions apart from the exchange, also break the invariance. The PMA leads to the energy increase with λ thus it should lead to a collapse. However, the dipole-dipole interaction favors the skyrmion expansion and, together with the PMA, it can stabilize the skyrmion at a particular size. DMI favors skyrmion expansion and adjustment of the chirality angle to a particulr value ($\gamma=\pi/2$ for the Bloch DMI with $A>0$). This expansion can be limited by the magnetic field applied in the negative direction with respect to the skyrmion's spin. This stabilizes the skyrmion at a particular size. If the applied field becomes too strong, the skyrmion collapses.

Certainly, the shape of the skyrmion stabilized by non-exchange interactions differs from the BP shape. However, since the exchange is the strongest interaction, at least small skyrmions are only weakly distorted. Thus, if makes sense to use Eq. (3) as the Ansatz in the analytical approach. Below, we will ignore the DDI and mainly investigate the model with the DMI, numerically and analytically, focusing on the breathing mode.

Breathing mode is the lowest-frequency local mode of the skyrmion in which the skyrmion size is oscillating around its equilibrium value. As we will see, this is accompanied by oscillations of the dynamically conjugate variable, the chirality angle γ. There should be faster modes including various deformations of the skyrmion, that will not be investigated.

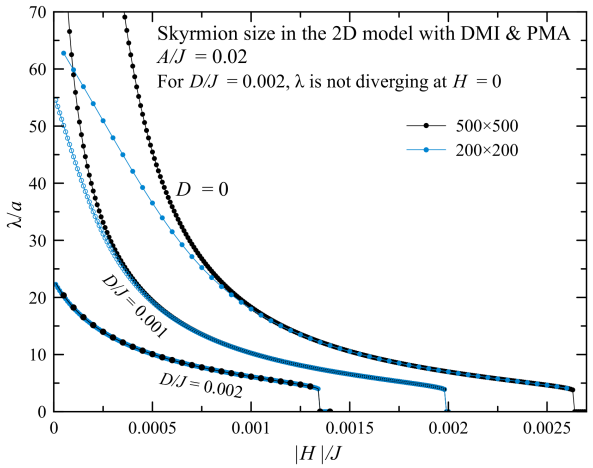


FIG. 2: Skyrmion size vs the applied magnetic field for $A/J = 0.02$ and different PMA values.

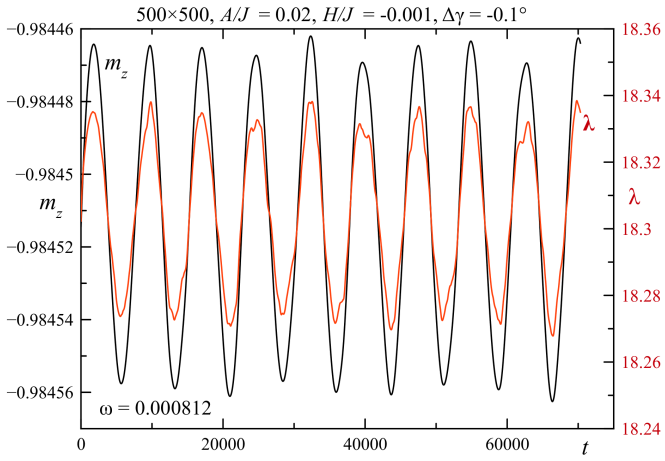


FIG. 3: Numerically obtained oscillations of m_z and of the skyrmion size λ in the breathing mode.

B. Numerical energy minimization and the skyrmion size

To find the frequency of the breathing mode numerically, first the energy minimization was done for a particular set of parameters. The main choice was $A/J = 0.02$, whereas the applied field H changed between its collapse value and zero. As the initial condition, any bubble with $Q = 1$ at the center of the system can be used. The numerical method [31] combines sequential rotations of spins $\mathbf{s}_i$ towards the direction of the local effective field, $\mathbf{H}_{\text{eff},i} = -\partial\mathcal{H}/\partial\mathbf{s}_i$, with the probability α, and the energy-conserving spin flips (overrelaxation), $\mathbf{s}_i \to 2(\mathbf{s}_i \cdot \mathbf{H}_{\text{eff},i})\mathbf{H}_{\text{eff},i}/H^2_{\text{eff},i} - \mathbf{s}_i$, with the probability $1-\alpha$. We used $\alpha = 0.03$ that ensures the fastest relaxation. It was found that the breathing mode can be seen only in the model with periodic boundary conditions (pbc), both for the exchange and for the DMI. In the case of free boundary conditions, there are surface modes that interfere in the extraction of the frequency of the breathing mode. Thus, all computation were performed on the model with pbc.

The skyrmion size λ can be extracted from the numerical data as [12]

$$\lambda_n^2 = \frac{n-1}{2^n\pi} a^2 \sum_i (s_{iz}+1)^n \,, \tag{4}$$

in our case $s_{iz} = -1$ in the background and $s_{iz} = 1$ at the center of the skyrmion. For the BP skyrmions with s_z given by Eq. (3), one has $\lambda_n = \lambda$ for any n. In this paper, we used $\lambda = \lambda_4$ to represent the numerically computed skyrmion size. We also computed the components of the average spin of the system as

$$\mathbf{m} = \frac{1}{N}\sum_i \mathbf{s}_i. \tag{5}$$

One can also define the skyrmion spin as

$$\mathcal{M} = \sum_i (s_{iz}+1)\,. \tag{6}$$

The angle γ was extracted by building the sum of dot products of the lattice spins $\mathbf{s}_i$ by the radial vectors $\mathbf{r}_i$ (with respect to the center of the lattice), that yields $\cos\gamma$, and by the $\boldsymbol{\phi}_i$-vectors, that are perpendicular to the $\mathbf{r}_i$-vectors and point counterclockwise, to find $\sin\gamma$.

The results for the equilibrium skyrmion size vs H for two different system sizes, $A/J = 0.02$, and three different values of the PMA, $D/J = 0$, 0.001, and 0.002, are shown in Fig. 2. For $D = 0$, the skyrmion size diverges in the limit $H \to 0$. However, the divergence is limited by the system size that is clearly seen in the figure. Thus, for a small field, a large system size is needed. PMA tends to decrease the skyrmion size, thus for $D/J = 0.001$ the latter is noticeably smaller, while the collapse field is smaller, too. The skyrmion size still diverges for $H \to 0$. To the contrary, for a stronger PMA, $D/J = 0.002$, the skyrmion size does not diverge and the results for both system sizes are the same. This means that a sufficiently strong PMA can stabilize the skyrmion at $H = 0$. On the other hand, if the PMA becomes too strong, the skyrmion will collapse. Thus, there is a range of D that stabilize the skyrmion at $H = 0$.

C. Numerical dynamics of the breathing mode

After the equilibrium skyrmion configuration was found, the frequency of its oscillations around the equilibrium was measured by running the dynamical evolution following the rotation of all spins in the system by $\Delta\gamma = 1°$ around the z-axis. We used the fourth-order Runge-Kutta ordinary-differential-equation solver with the integration step 0.2 in the units of $\hbar/J$ to solve the

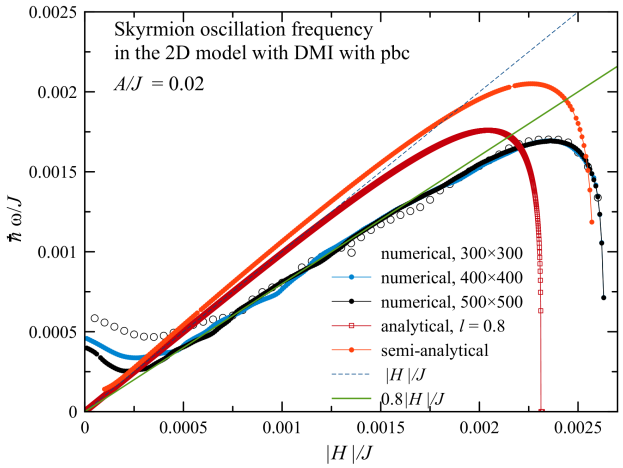


FIG. 4: Field dependence of the oscillation frequency of the breathing mode computed numerically on lattices of different sizes, analytically for a BP skyrmion shape with logarithmic accuracy, and semi-analytically in a model with the skyrmion shape corrected, see Section III.

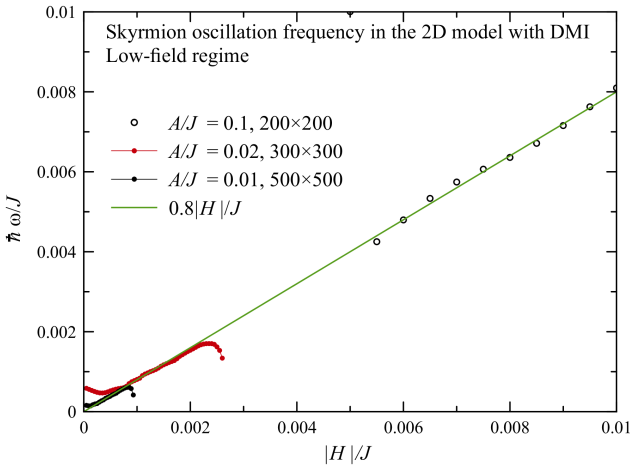


FIG. 5: Frequency of the breathing mode in the linear-H regime for different values of the DMI constant A.

system of Larmor equations of motion $\hbar\dot{\mathbf{s}}_i = \mathbf{s}_i \times \mathbf{H}_{\text{eff},i}$ for the lattice spins. No damping was included in this computation. For the small DMI constant and the applied field used here, the dynamics is rather slow, so that the discretization error of the Runge-Kutta method is rather small. However, one cannot significantly increase the step as already for the step 0.3 an instability occurs due to the exchange term in the equations.

The computation was done independently for each value of H in parallel using Worfram Mathematica with vectorization and compilation on a 20-core Dell Precision Workstation (16 cores used by Mathematica). Computations performed for $A/J = 0.1$, 0.02, 0.01 show qualitatively similar behavior. In the paper the results are given for $A/J = 0.02$ with $D/J = 0$ and $D/J = 0.002$. They were computed for the system sizes 100×100, 200×200, 300×300, 400×400, and 500×500. A greater system size is needed for small applied fields when the skyrmion size becomes large. Comparison of the results for different system sizes show that at our maximal size 500×500 there are no finite-size effects in the main range of H, except for the smallest H.

It was found that the skyrmion size λ and the system's average spin m_z (or, equivalently, the skyrmion's magnetic moment $\mathcal{M}$) performed periodic oscillations with a weak anharmonicity, see Fig. 3. Since the curves for m_z are smoother than those for λ, the former were used to extract the oscillation frequency. The anharmonicity could be attributed to a weak hybridization of the breathing mode with the other local modes (see, e.g., Ref. [32]) that also could be excited by rotating all spins by $\Delta\gamma$. Indeed, the deviation from the equilibrium skyrmion state can be expanded over the set of local modes. In this expansion, the breathing mode should be the strongest while other modes enter with smaller weights and thus they distort the breathing dynamics to some extent seen in the dependences $\lambda(t)$ and $m_z(t)$. On the other hand, no damping of the breathing mode was detected. This can be explained by the fact that its frequency always falls below the frequency of the uniform precession, that is, the breathing mode is not resonating with the spin-wave band. The time interval between the adjacent maximum and minimum (or between a minimum and a maximum) of m_z was interpreted as the half of the period to extract the oscillation frequency. This half-period of the evolution costs much more computer time than finding the skyrmion's equilibrium state in the first stage. In the parallelized computation for diffeent values of H, after reaching the first maximum and the first minimum of m_z, the computation was terminated and the frequency was recorded.

The dependence of the frequency of the breathing mode on the magnetic field at $D = 0$ is shown in Fig. 4. The $\omega(H)$ curves obtained numerically on lattices of different size have little size dependence, except for weak fields, where $\omega(H)$ has a size-dependent uptick. Here one can expect skyrmions branching out and transform to a laminar domain state. The $\omega(H)$ curves exhibit a characteristic maximum on approach to the critical field above which the skyrmion collapses. Here $\omega(H)$ goes to zero steeply. On the left side of the maximum, where skyrmions are big and the lattice discreteness becomes unimportant, $\omega(H)$ goes apparently linearly and can be approximated by the dependence $\hbar\omega(H) = 0.8H$. Qualitatively similar behavior is exhibited by the $\omega(H)$ curves computed analytically in the next Section, that are shown in the same figure.

It is remarkable that the dependence $\hbar\omega(H) = 0.8H$ holds for different values of the DMI constant A. Thus, the coefficient 0.8 is a universal number.

Numerical results in the presence of the PMA are

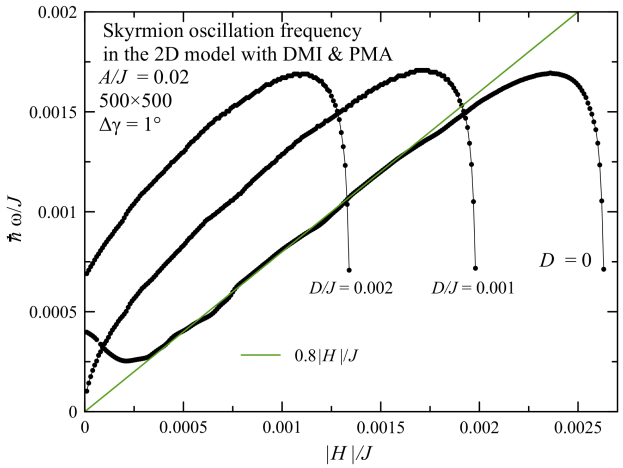


FIG. 6: Breathing-mode frequency vs the applied magnetic field for $A/J = 0.02$ and different PMA values for the 500×500 system size.

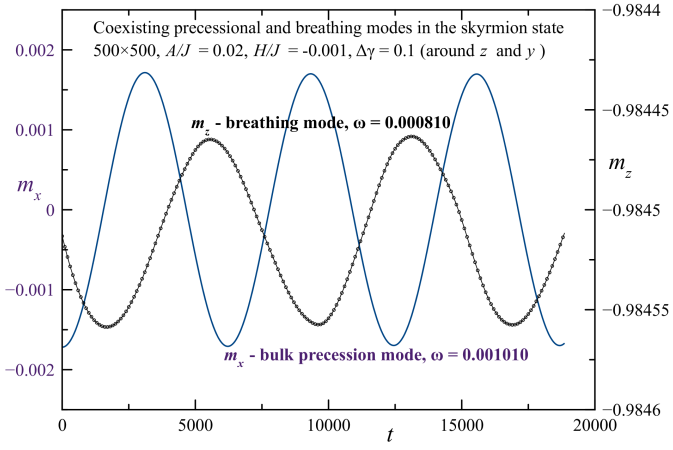


FIG. 7: Coexisting breathing and bulk precession modes after rotating spins around z- and y-axes out of the equilibrium-skyrmion state. These modes oscillate at close but distinctly different frequences.

shown in Fig. 6 for $A/J = 0.02$ and the system size 500×500. In accordance with Fig. 2, the collapse fields and the entire curves shift to the left with increasing the PMA. The breathing-mode frequency $\omega(H)$ is well below the FMR frequency $\omega_{\rm FMR} = (D + H)/\hbar$. For $D/J = 0.001$, $\omega(H)$ goes to zero with a high slope at $H \to 0$. This must be related to the divergence of $\lambda(H)$ seen in Fig. 2. To the contrary, for $D/J = 0.002$, the breathing-mode frequency remains finite at $H = 0$ that correlates with the finite λ at zero field in Fig. 2.

It is non-trivial that at $D = 0$ the frequency of the breathing mode in the main region of the applied field follows, for any value of A, a linear law $\hbar\omega(H) = 0.8H$ that is resembling that for the FMR frequency $\hbar\omega_{\rm FMR} = H$

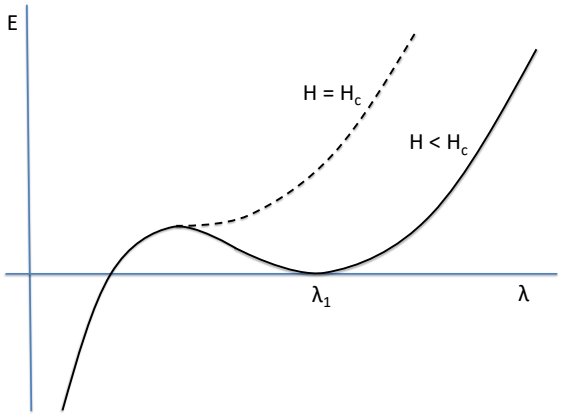


FIG. 8: Dependence of the skyrmion energy on skyrmion size λ for $\gamma = \pi/2$. The minimum corresponding to the equilibrium size disappears for $H > H_c$. At $H = H_c$ the energy has an inflection point where both first and second derivative are zero.

but has a smaller coefficient. In fact, the breathing mode and the bulk-precession mode have totally different structures. In the precession mode, $m_z = \text{const}$ while m_x and m_y are precessing. In the breathing mode, m_z is oscillating, while the spin orientation quantified by the angle γ is performing small oscillations around its equilibrium value. These two main modes are independent at small amplitudes and can coexist. To check this, we initiated dynamics by rotating all spins by 0.1° around the y- and z-axes. This excites both modes, the temporal evolution of which is shown in Fig. 7. One can see that the frequencies of these modes are different. Moreover, rotation of spins only around the z-axis, to excite the breathing mode, also excites the bulk precession mode with a very small, although numerically detectable amplitude, evolving with the proper FMR frequency.

III. SKYRMION BREATHING MODE IN A SPIN-FIELD MODEL

A. Analytical approach with the BP Ansatz for the skyrmion shape

The fact that $\omega(H)$ tends to zero at the critical field, $H = H_c$, can be easily understood from the dependence of the energy on the field and the size of the skyrmion shown in Fig. 8. Skyrmion of a stable size exists at $H > H_c$ when $E(\lambda)$ has a minimum. At $H = H_c$ the minimum becomes an inflection point where both, first and second derivative of E on λ, are zero. It is the nullification of the second derivative that makes the frequency of the breathing mode zero at $H = H_c$. In this Section we develop analytical approach that elucidates the dynamics of the breathing mode in simple physical terms.

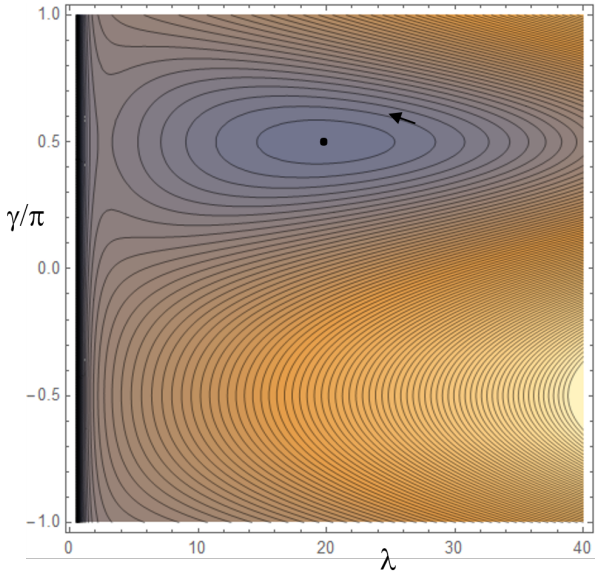


FIG. 9: Equipotential lines in the $\{\lambda, \gamma\}$ plane corresponding to Eq. (8) with $l = \text{const}$.

The continuous analog of Eq. (1) is

$$\begin{aligned}\mathcal{H} &= \frac{JS^2}{2}\int dxdy\left[\left(\frac{\partial \mathbf{s}}{\partial x}\right)^2+\left(\frac{\partial \mathbf{s}}{\partial y}\right)^2\right]\\ &- \frac{JS^2a^2}{24}\int dxdy\left[\left(\frac{\partial^2 \mathbf{s}}{\partial x^2}\right)^2+\left(\frac{\partial^2 \mathbf{s}}{\partial y^2}\right)^2\right]\\ &- \frac{HS}{a^2}\int dxdy\, s_z - \frac{DS^2}{2a^2}\int dxdy\, s_z^2\\ &+ \frac{AS^2}{a}\int dxdy\left[\left(\mathbf{s}\times\frac{\partial \mathbf{s}}{\partial x}\right)\cdot\mathbf{e}_x+\left(\mathbf{s}\times\frac{\partial \mathbf{s}}{\partial y}\right)\cdot\mathbf{e}_y\right] \quad (7)\end{aligned}$$

The second term in this expression arises from taking into consideration the next derivatives in the expansion of the discrete form of the exchange energy that dominates spin interactions at small distances. The spin combination in the DMI energy can be rewritten as $\mathbf{s}\cdot(\nabla\times\mathbf{s})$. For a small skyrmion that is close to the BP shape, substitution of Eq. (3) into Eq. (7) gives at $D = 0$

$$\bar{E} \equiv \frac{\mathcal{H}}{4\pi JS^2} = h\bar{\lambda}^2 l(\bar{\lambda}) - \frac{1}{6\bar{\lambda}^2} - \alpha\bar{\lambda}\sin\gamma, \quad (8)$$

where $h \equiv H/(JS)$, $\alpha \equiv A/J$, $\bar{\lambda} \equiv \lambda/a$, and $l(\bar{\lambda})$ has a logarithmic dependence on λ that is sensitive to the shape of the skyrmion far from its center. This function for $\gamma = \pi/2$ is shown qualitatively in Fig. 8.

Consider first a crude approximation with $l = \text{const}$. The whole potential landscape of Eq. 8 is shown in Fig. 9 for $\alpha = 0.02$, $h = -0.001$, and $l = 0.5$. As the dynamics of the skyrmion conserves the energy, the system is moving in its phase space $\{\lambda, \gamma\}$ along the equipotential lines. The motion occurs in the counterclockwise direction. The center point is the energy minimum $\gamma = \pi/2$ and $\lambda = \lambda_1$ defined by the angebraic equation

$$\frac{\partial \bar{E}}{\partial \bar{\lambda}} = 2lh\bar{\lambda} + \frac{1}{3\bar{\lambda}^3} - \alpha = 0. \quad (9)$$

There are two regimes of the breathing motion of the skyrmion, if one looks at the behavior of γ. The oscillating regime corresponds to closed trajectories around the metastable energy minimum. The rotating regime is described by γ steadily increasing with time. However, one can reduce γ to the interval $(-\pi, \pi)$. In this representation, in the rotating regime trajectories are leaving the area through the top and reentering through the bottom. The skyrmion size λ is oscillating in both regimes.

Solution of Eq. (9) together with the equation $\partial^2\bar{E}/\partial\bar{\lambda}^2 = 2lh - 1/\bar{\lambda}^4 = 0$ gives the critical field, h_c, and the value of $\bar{\lambda}_1 = \bar{\lambda}_c =$ at the critical field,

$$h_c = \frac{1}{2l}\left(\frac{3\alpha}{4}\right)^{4/3}, \qquad \bar{\lambda}_c = \left(\frac{4}{3\alpha}\right)^{1/3}. \quad (10)$$

At $h \ll h_c$ one has $\bar{\lambda}_1 \approx \alpha/(2lh)$. This roughly agrees with the lattice results shown in Fig. 4.

To study the dynamics of the spin system, consider the Lagrangian [20]

$$\mathcal{L} = \hbar S\int dxdy\dot{\Phi}(\cos\Theta + 1) - \mathcal{H}, \quad (11)$$

where Θ and Φ are spherical coordinates of $\mathbf{S}$, satisfying $\cos\Theta + 1 = s_z + 1$ and $\tan\Phi = s_y/s_x$. Substituting here Eq. (3), which results in $\dot{\Phi} \equiv d\Phi/dt = \dot{\gamma}$, upon integration one obtains

$$\mathcal{L} = 4\pi\hbar S\dot{\gamma}\bar{\lambda}^2 l - E(\bar{\lambda}, \gamma). \quad (12)$$

The Euler-Lagrange equations are

$$\frac{\partial \mathcal{L}}{\partial \bar{\lambda}} = 0, \qquad \frac{d}{dt}\frac{\partial \mathcal{L}}{\partial \dot{\gamma}} = \frac{\partial \mathcal{L}}{\partial \gamma}, \quad (13)$$

resulting in the coupled equations of motion for $\bar{\lambda}$ and γ:

$$2\frac{d\gamma}{dt}\bar{\lambda}l = -\alpha\sin\gamma + 2h\bar{\lambda}l + \frac{1}{3\bar{\lambda}^3} \quad (14)$$

$$2\frac{d\lambda}{dt}l = \alpha\cos\gamma. \quad (15)$$

Linearization of the above equations for small amplitude oscillations yields the frequency of the breathing mode,

$$\bar{\omega}_1(h) = \frac{\hbar\omega}{JS} = \frac{\alpha^{1/2}}{2l\bar{\lambda}_1^{1/2}}\sqrt{2lh - \frac{1}{\bar{\lambda}_1^4}}, \quad (16)$$

where $\bar{\lambda}_1(h)$ is given by Eq. (9). Its dependence on the magnetic field for $l = 0.8$ is shown in Fig. (4).

It is easy to see that at $h \ll h_c$ the above equation gives $\bar{\omega}_1 = h[1-(\bar{\lambda}_c/\bar{\lambda}_1)^3/4] \approx h$. This coincides with the FMR frequency and differs from a more accurate numerical lattice result $\bar{\omega}_1 \approx 0.8h$ that brings the frequency of the

breathing mode below the bottom of the spin-wave spectrum in the bulk. The latter does not allow the breathing mode to decay into spin waves and is responsible for its non-dissipative dynamics if damping from other sources is not introduced by hand into the equations of motion.

The above method relies on a fitting parameter l to come close to the numerically obtained critical field. Although this simple method provides a physical picture of the breathing-mode dynamics and provides qualitatively correct results including the maximim of the breathing-mode frequency, there are discrepancies with the numerical solution both near the skyrmion collapse and at low fields.

B. Semi-analytical approach using corrected skyrmion shape

A better approximation not using any fitting parameters can be developed if one takes into account the deformation of the BP shape of the skyrmion at large distances. Because of the applied field H, the spin field approaches its background value -1 exponentially at the magnetic length $\delta_H = \sqrt{JS/|H|}$. In the limit $\lambda \ll \delta_H$, the asymptotic solution of the linearized equation for $\mathbf{s}(\mathbf{r})$ at $r \gg \lambda$ can be combined with the BP solution at $r \ll \delta_H$. This leads to replacement of Eq. (3) by

$$\left\{ \begin{array}{c} s_x \\ s_y \end{array} \right\} = \frac{2\lambda f(r)}{f^2(r)+\lambda^2} \left\{ \begin{array}{c} \cos(\phi+\gamma) \\ \sin(\phi+\gamma) \end{array} \right\}, \quad s_z = \frac{\lambda^2 - f^2(r)}{\lambda^2 + f^2(r)}, \tag{17}$$

where $f(r) = \delta_H / K_1(r/\delta_H)$ and K_1 is the MacDonald function (see, e.g, Ref. [19]). Although formally valid for $\lambda \ll \delta_H$, this solution that rescales the distance from the skyrmion's center proves to be remarkably robust and provides good results in a wide range of H. The reason is that the actual skyrmion profile obtained numerically or within this approximation, always satisfies $\lambda \lesssim \delta_H$, whereas the opposite limit is never realized.

Substitution of Eq. (17) into Eq. (11) gives

$$\mathcal{L} = \hbar\dot{\gamma}\mathcal{M}(\lambda) - E(\lambda,\gamma), \tag{18}$$

where

$$\mathcal{M}(\lambda) = \int dxdy \frac{2\lambda^2}{f^2(r)+\lambda^2} \tag{19}$$

is the magnetic moment of the skyrmion and $E(\lambda,\gamma)$ is the energy (7) corresponding the modified profile of the skyrmion.

The coupled equations of motion for $\mathcal{M}$ and γ that follow from Eq. (13) are

$$\hbar\frac{d\gamma}{dt}\frac{d\mathcal{M}}{d\lambda} = \frac{dE}{d\lambda}, \quad \hbar\frac{d\lambda}{dt}\frac{d\mathcal{M}}{d\lambda} = -\frac{dE}{d\gamma}. \tag{20}$$

For small oscillations, $\delta\lambda$ and $\delta\gamma$, near their equilibrium values $\delta\lambda_1$ and $\delta\gamma_1$, approximating the energy by a parabolla,

$$E(\lambda,\gamma) = E(\lambda_1,\gamma_1) + \frac{1}{2}E_{\lambda\lambda}\delta\lambda^2 + \frac{1}{2}E_{\gamma\gamma}\delta\gamma^2, \tag{21}$$

one obtains linear equations of motion

$$\frac{d\delta\gamma}{dt} = \frac{E_{\lambda\lambda}}{\hbar\mathcal{M}_\lambda}\delta\lambda, \quad \frac{d\delta\lambda}{dt} = -\frac{E_{\gamma\gamma}}{\hbar\mathcal{M}_\lambda}\delta\gamma, \tag{22}$$

where $E_{\lambda\lambda} \equiv \partial^2 E/\partial\lambda^2$, $E_{\gamma\gamma} \equiv \partial^2 E/\partial\gamma^2$, and $\mathcal{M}_\lambda \equiv d\mathcal{M}/d\lambda$. These equations describe the oscillating motion of the dynamically conjugate pair $\{\delta\lambda, \delta\gamma\}$ at a frequency

$$\omega = \sqrt{\frac{E_{\lambda\lambda}E_{\gamma\gamma}}{\hbar\mathcal{M}_\lambda}}. \tag{23}$$

This solution is more general than the one given above and it reproduces Eq. (16) if the BP skyrmion profile is used.

The energy $E(\lambda,\gamma)$ should now be computed numerically with the help of Eqs. (7), and (17) and minimized with respect to λ and γ to obtain their equilibrium values. This gives $\gamma = \pi/2$ as before. The corresponding shape and equilibrium size of the skyrmion computed that way and compared with numerical results on the lattice are illustrated in Fig. 10. Deviation from the BP shape at large distances from the center of the skyrmion is quite significant while disagreement between our semi-analytical model and numerical results obtained on the lattice is rather small.

A better agreement with numerical results on the lattice (achieved in the absence of any fitting parameter) can also be seen in the plot of $\omega(H)$ of Eq. (23) shown by red line in Fig. 4. In particular, the semi-analytical approach provides a much better description of the collapse region than the crude analytical approach. However, the correct slope 0.8 in the low-field $\omega(H)$ is not captured.

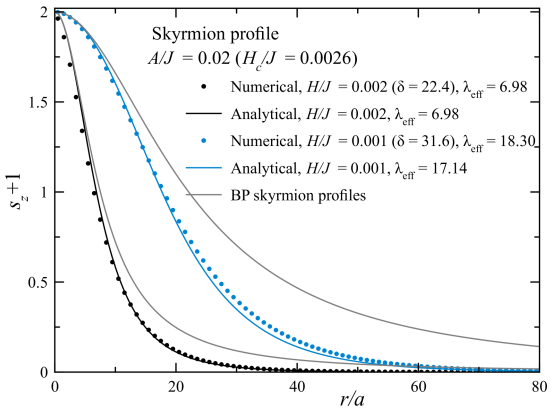


FIG. 10: Modified skyrmion shape given by Eq. (17) with the equilibrium size $\lambda_{\rm eff}$ obtained by the numerical minimization of the energy for two values of the magnetic field. Comparison with the BP shape and numerical results obtained on the lattice are also shown.

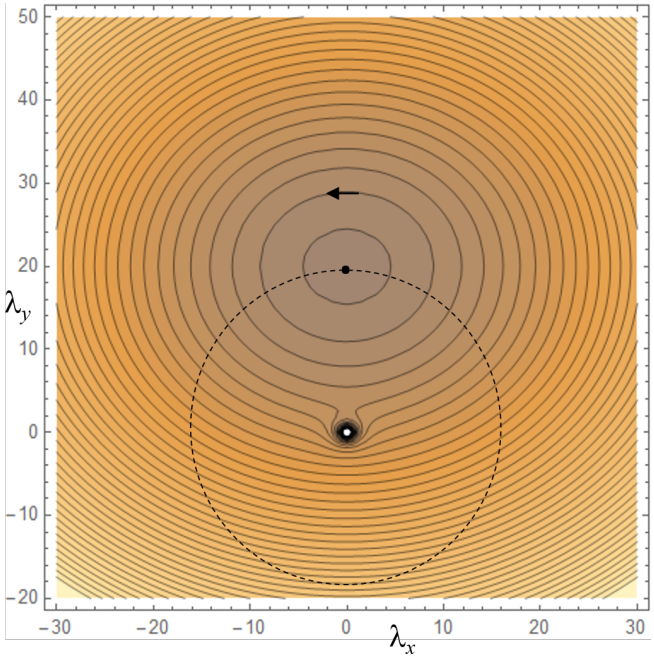


FIG. 11: Equipotential lines in the $\{\lambda_x, \lambda_y\} = \{\lambda\cos\gamma, \lambda\sin\gamma\}$ plane corresponding to Eq. (8) with $l = \text{const}$.

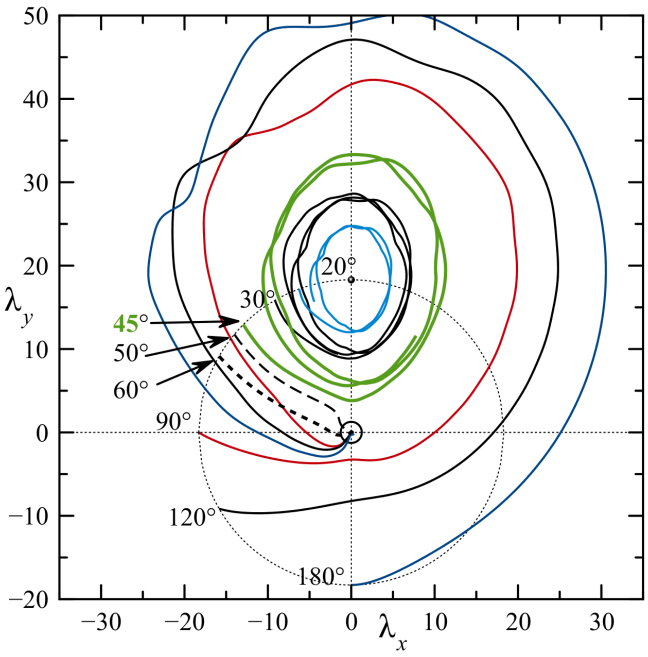


FIG. 12: Dynamics of the breathing mode after rotation of the spins by a large angle $\Delta\gamma$ in the system of 500×500 spins with $A/J = 0.02$ and $H/J = -0.001$. For $\Delta\gamma \gtrsim 50°$, the skyrmion collapses.

IV. LARGE-AMPLITUDE BREATHING MODE

In this section, we investigate numerically the dynamics of large amplitude breathing mode inititiated by rotating the spins by a large angle $\Delta\gamma$. Instead of the phase diagram in terms of $\{\lambda.\gamma\}$ shown in Fig. 9, it is more convenient to use the phase diagram in terms of $\{\lambda_x, \lambda_y\} = \{\lambda\cos\gamma, \lambda\sin\gamma\}$. For the same parameters as Fig. 9, this new phase diagram is shown in Fig. 11. Here, all equipotential lines are closed. Oscillating regime corresponds to equipotential lines that do not enclose the center $\{0, 0\}$ where the skyrmion collapses. Rotating regime corresponds to the lines that do enclose the center. Rotation of the spins by the angle $\Delta\gamma$ out of the equilibrium point denoted by the dot, corresponds to the displacement along the dashed circle around the center.

Numerical results in Fig. 12 show that stable breathing motion is possible for $\Delta\gamma < 45°$, although this motion is clearly affected by the coupling to other modes. For larger amplitudes, the skyrmion collapses approaching the collapse point either directly ($\Delta\gamma = 50°$ and $60°$) or after one rotation ($\Delta\gamma = 90°$, $120°$, and $180°$). Such a quick dissipation of the energy of the breathing mode should be due to the energy transfer into the other modes, whereas the total energy of the system is conserved. In fact, as the measured frequency of the large-amplitude breathing modes approaches the FMR frequency ($\omega = 0.000929$, 0.000988, and 0.0010649 for $\Delta\gamma = 90°$, $120°$, and $170°$, respectively), energy transfer into bulk precession mode becomes possible. This is not surprising because the rotational breathing mode evolves in the same direction, thus it can efficiently drive the bulk precession mode, losing its energy. To the contrary, motion of γ back and forth in the oscillating regime cannot drive the bulk precession mode. When the skyrmion collapses, its entire energy is converted into that of spin waves.

V. CONCLUSIONS

We have studied the breathing mode of a skyrmion stabilized by the Dzyaloshinskii-Moriya interaction in a non-centrosymmetric magnetic film. Compared to the previous studies our focus has been on large fields close to the stability threshold. In that region the frequency of the breathing mode reaches maximum on the field and then tends to zero on approaching the collapse field. This effect must exist not only for individual skyrmions but also for skyrmions forming a lattice. It should not be difficult to test in experiment.

The above behavior of the breathing mode has been obtained by three methods: Computations on lattices up to 500×500 in size; crude analytical approximation using the Belavin-Polyakov shape of the skyrmion; and a semi-analytical dynamical model based upon modified skyrmion shape. All three models have produced qualitatively same behavior and agree with each other quantita-

tively within 20%. Analytical approach provides a simple picture of the breathing mode as coupled oscillations of the skyrmion size and magnetic moment.

The most accurate numerical model on the lattice shows that the frequency of the breathing mode in the oscillating regime is always below the excitation spectrum in the bulk and, thus, it cannot decay into spin waves. This explains why no damping of the breathing oscillation of the skyrmion has been observed in the numerical experiment within the conservative spin model. In real experiments the damping may result from coupling to phonons and conducting electrons. It is expected to be weak in insulating materials. On the other hand, in the rotating regime the frequency of the breathing mode increases and it becomes strongly damped apparently via energy transfer into the bulk precession mode. Unlike the long-wavelength undamped micromagnetic approach, the lattice-based nonlinear dynamics used here captures all scales of excitations up to the atomic scale ($ka \sim 1$), thus it describes the processes of natural damping in the absence of damping added "by hand". In that approach the short-wavelength spin waves serve as the main energy reservoir for the relaxation.

Current induced spin torques have been used to manipulate skyrmions [7]. In such experiments the breathing dynamics could be used to control skyrmion trassport through a constriction [6]. If skyrmions are utilized for data storage and processing, our theory developed for the smallest skyrmions must be useful for analyzing their response to external perturbations.

VI. ACKNOWLEDGMENTS

This work has been supported by the grant No. DE-FG02-93ER45487 funded by the U.S. Department of Energy, Office of Science.

[1] N. Nagaosa and Y. Tokura, Nature Nanotechnology **8**, 899-911 (2013).
[2] R. Tomasello, E. Martinez, R. Zivieri, L. Torres, M. Carpentieri, and G. Finocchio, Nature Scientific Reports **4**, 6784-(7) (2014).
[3] X. Zhang, M. Ezawa, and Y. Zhou, Scientific Reports **5**, 9400-(8) (2015).
[4] G. Finocchio, F. Büttner, R. Tomasello, M. Carpentieri, and M. Klaui, Journal of Physics D: Applied Physics. **49**, 423001-(17) (2016).
[5] A. O. Leonov, T. L. Monchesky, N. Romming, A. Kubetzka, A. N. Bogdanov, and R. Wiesendanger, New Journal of Physics **18**, 065003-(16) (2016).
[6] W. Jiang, G. Chen, K. Liu, J. Zang, S. G. E. te Velthuis, and A. Hoffmann, Physics Reports **704**, 1 - 49 (2017).
[7] A. Fert, N. Reyren, and V. Cros, Nature Reviews Materials **2**, 17031-(15) (2017).
[8] T. H. R. Skyrme, Proceedings of the Royal Society A **247**, 260-278 (1958).
[9] N. Manton and P. Sutcliffe, *Topological Solitons*, Cambridge University Press 2004.
[10] A. A. Belavin and A. M. Polyakov, Pis'ma Zh. Eksp. Teor. Fiz **22**, 503-506 (1975) [Sov. Phys. JETP Lett. **22**, 245-248 (1975)].
[11] E. M. Chudnovsky and J. Tejada, *Lectures on Magnetism*, Rinton Press (Princeton - NJ, 2006).
[12] L. Cai, E. M. Chudnovsky, and D. A. Garanin, Physical Review B **86**, 024429 (2012).
[13] F. Buttner, I. Lemesh, and G. S. D. Beach, Sci. Rep. **8**, 4464 (2018).
[14] O. Boulle, J. Vogel, H. Yang, S. Pizzini, D. S. de Souza Chaves, A. Locatelli, T. O. Mentes, A. Sala, L. D. Buda-Prejbeanu, O. Klein, M. Belmeguenai, Y. Roussigné, Y. A. Stashkevich, S. M. Chérif, L. Aballe, M. Foerster, M. Chshiev, S. Auffret, I. M. Miron, and G. Gaudin, Nature Nanotechnology **11**, 449 (2016).
[15] C. Moreau-Luchaire, C. Moutas, N. Reyren, J. Sampaio, C. A. F. Vaz, N. Van Horne, K. Bouzehouane, C. Garcia, K. Deranlot, P. Warnicke, P. Wohlhter, J.-M. George, M. Weigand, J. Raabe, V. Cros, and A. Fert, Nature Nanotechnology **11**, 444 (2016).
[16] N. Romming, C. Hanneken, M. Menzel, J. E. Bickel, B. Wolter, K. von Bergmann, A. Kubetzka, and R. Wiesendanger, Science **341**, 636 (2013).
[17] Romming, N., A. Kubetzka, C. Hanneken, K. von Bergmann, and R. Wiesendanger, Physical Review Letters **114**, 177203 (2015).
[18] E. B. Kaufluss and U.-G. Meissner, Physics Letters **154B**, 193 (1985).
[19] V. P. Voronov, B. A. Ivanov, and A. M. Kosevich, Zh. Eksp. Teor. Fiz. **84**, 2235 (1983) [Sov. Phys. JETP **57**, 1303 (1983)].
[20] A. Derras-Chouk, E. M. Chudnovsky, and D. A. Garanin, Physical Review B **98**, 024423-(9) (2018).
[21] T. H. O'Dell, *Ferromagnetodynamics: The Dynamics of Magnetic Bubbles, Domains, and Domain Walls* (Wiley - 1981).
[22] See for review: M. Garst, J. Waizner, and D. Grundler, Journal of Physics D: Applied Physics **50**, 293002 (2017).
[23] M. Mochizuki, Physical Review Letter **108**, 017601 (2012).
[24] I. Makhfudz, B. Kruger, and O. Tchernyshyov, Physical Review Letters **109**, 217201 (2012).
[25] Y. Onose, Y. Okamura, S. Seki, S. Ishiwata, and Y. Tokura, Physical Review Letters **109**, 037603 (2012).
[26] S.-Z. Lin, C. D. Batista, and A. Saxena, Physical Review B **89**, 024415 (2014).
[27] J-V. Kim, F. Garcia-Sanchez, J. Sampaio, C. Moreu-Luchaire, V. Cros, and A. Fert, Physical Review B **90**, 064410 (2014).
[28] S.-Z. Lin, Physical Review B **96**, 014407 (2017).
[29] V. P. Kravchuk, D. D. Sheka, U. K. Robler, J. van der Brink, and Y. Gaididei, Physical Review B **97**, 064403 (2018).
[30] B. F. McKeever, D. R. Rodriguez, D. Pinna, A. Abanov, J. Sinova, and K. Everschor-Sitte, Physical Review B **99**, 054430 (2019).
[31] D. A. Garanin, E. M. Chudnovsky, and T. Proctor, Phys-

ical Review B **88**, 224418 (2013).
[32] L. Desplat, D. Suess, J-V. Kim, and R. L. Stamps, Physical Review B **98**, 134407 (2018).